IEEE Access
Multidisciplinary ⋮ Rapid Review ⋮ Open Access Journal

Received 1 October 2023, accepted 24 October 2023, date of publication 27 October 2023, date of current version 2 November 2023.

Digital Object Identifier 10.1109/ACCESS.2023.3328241

RESEARCH ARTICLE

Selective Locomotion Control of Magnetic Torque-Driven Magnetic Robots Within Confined Channels

ARMANDO RAMOS-SEBASTIAN[1], (Member, IEEE), WONSUK JUNG[2], AND SUNG HOON KIM[3], (Member, IEEE)

[1]Sejong Research and Business Foundation, Korea University, Sejong 30019, Republic of Korea
[2]School of Mechanical Engineering, Chungnam National University, Daejeon 34134, Republic of Korea
[3]Department of Electronics and Information Engineering, Korea University, Sejong 30019, Republic of Korea

Corresponding authors: Wonsuk Jung (wonsuk81@cnu.ac.kr) and Sung Hoon Kim (kshoon04@korea.ac.kr)

This work was supported in part by the Korea Medical Device Development Fund through the Korean Government (Ministry of Science and ICT, Ministry of Trade, Industry and Energy, Ministry of Health and Welfare, and Ministry of Food and Drug Safety) under Project KMDF_PR_20200901_0130, 1711138241; in part by the National Research Foundation of Korea (NRF) grant funded by the Korean Government (MSIT) under Grant 2022R1A2C1003381; and in part by the Basic Science Research Program through NRF funded by the Ministry of Education under Grant NRF-2022R1I1A3069079.

ABSTRACT The use of global magnetic fields—typically produced by pairs of Maxwell and Helmholtz coils—offers the advantage of generating uniform magnetic fields and magnitude uniform gradient distributions over extensive volumes, while ensuring easy control. However, achieving selective control of multiple magnetic microrobots under such global fields remains problematic. In this study, we utilize a magnetic focus field generated by a pair of Maxwell coils to impede the magnetic torque-based movement of magnetic robots confined within channels. Although the magnetic field is null at the focus field's center, it increases linearly in all directions. This exerts magnetic forces that push robots, which are situated away from the center, toward the channel walls. This not only restricts their positioning but also reduces their responsiveness to additional fields. By introducing uniform dc magnetic fields to the focus field, we can change the controlled robot. This mechanism for selective locomotion has been empirically validated with the selective movement of two helical magnetic robots and swarms of magnetic microparticles. Furthermore, leveraging the same focus field, we present a novel separation mechanism for magnetic particle swarms, enhancing the aforementioned selective locomotion mechanism. The practical implications of our proposed locomotion mechanism have been showcased in targeted delivery, drilling, and improved magnetic heating experiments.

INDEX TERMS Electromagnetic system, magnetic microrobots, magnetic nanoparticles, magnetic heating, selective locomotion.

I. INTRODUCTION

Since their inception, magnetic-driven robots (hereinafter referred to as magbots) have been extensively researched due to their wireless power, control, and potential for miniaturization down to the micro/nano scale. These qualities make them suitable for a plethora of biomedical applications, including embolization [1], [2], drug delivery [3], [4], and hyperthermia [5], [6]. As a result, a variety of electromagnetic control systems have been developed for manipulating these magbots. These range from systems that utilize permanent magnets manipulated by robotic arms and platforms [7], [8], [9], to those employing static [10], [11] or moving electromagnets [12], [13]. Additionally, several magnetic torque-based locomotion mechanisms for magbots have been proposed [14]. Notwithstanding, controlling magbots often remains limited to either a single robot or to the collective control of multiple robots that aren't individually addressable. This limitation arises from the challenges associated with producing distinct magnetic fields at various locations within a

The associate editor coordinating the review of this manuscript and approving it for publication was Yangmin Li.

workspace to enable the independent operation of multiple robots.

To date, the most effective method for controlling multiple identical magbots employs arrays of electromagnets [15], [16]. This approach, however, necessitates a significant number of coils. The quantity of these coils tends to increase in tandem with the system's working volume and resolution. Moreover, this technique is generally constrained to two-dimensional applications. Some researchers have offered alternative solutions by employing magbots with distinct geometries [17] or by altering their magnetic moments through modifications in magnetic volume [18], magnetization direction [19], or magnetic material composition [20]. This ensures each magbot responds uniquely to a universally applied magnetic field distribution (or global fields). While the number of robots controlled through this method is typically limited (often fewer than five), its primary advantage lies in its applicability under global fields, facilitating three-dimensional movement.

Global fields are typically produced by pairs of Helmholtz and uniform saddle coils for the generation of space-uniform magnetic fields. In contrast, pairs of Maxwell and gradient saddle coils are employed for producing magnitude constant gradient fields over expansive volumes [21], [22], [23]. Utilizing these coil pairs, scholars have successfully controlled identical helical micromachines within threaded plates, demonstrating 1 Degree of Freedom (DoF) [24]. Similarly, they have controlled swarms of magnetic nanoparticles situated in distinct channels, also exhibiting only 1 DoF [25]. This is achieved by establishing a substantial gradient field with pairs of Maxwell coils, which attenuates the response of magnetic materials positioned away from the center of the Maxwell coil pairs to an added rotating magnetic field (RMF).

This study introduces an innovative locomotion mechanism for the individual control of torque-based magnetic robots (magbots) within confined channels. This is realized using global fields generated by pairs of Maxwell coils and a triaxial system of Helmholtz coil pairs. Selective locomotion is attained by harnessing the magnetic force from the Maxwell coils, which drives the magbots against the channel walls, thereby anchoring their position. Additionally, their reaction to supplementary low RMFs, produced by the Helmholtz coils, is subdued due to the notably high magnetic field output of the Maxwell coils when situated far from the coil's center. This inhibits their magnetic torque-driven movement. The presented locomotion approach is exemplified through the selective movement of two identical helical swimmers and a swarm of magnetic particles. A unique split mechanism for magnetic nanoparticle (MNP) swarms, which leverages the same magnetic gradient distribution from the Maxwell coils, is also introduced and validated. Furthermore, for the first time, the selective movement of entirely distinct magbots, in terms of both geometry and magnetic composition, is showcased. This is manifested through the precise control of helical magbots and MNP swarms for tasks such as drilling, delivery, and enhanced magnetic heating applications.

II. SELECTIVE LOCOMOTION MECHANISM

The process to achieve selective locomotion of magnetic torque-based magnetic robots is divided into two main steps: Firstly, the generation of a focus field (FF) and a selection volume (V_s); and, secondly, the V_s position control and selective actuation. V_s is a magnetic field distribution describing an imaginary ellipsoidal volume. Within this volume, the magnetic field undergoes complete rotations. In contrast, outside the ellipsoid, the field's oscillation is limited to a few degrees, impeding a full rotation. This distinction is critical in the context of magnetic torque-based magbots. Only a magbot positioned within the Vs domain can achieve full rotation, enabling effective propulsion. V_s is generated through the concurrent application of an FF and an RMF, as delineated in Fig. 1.

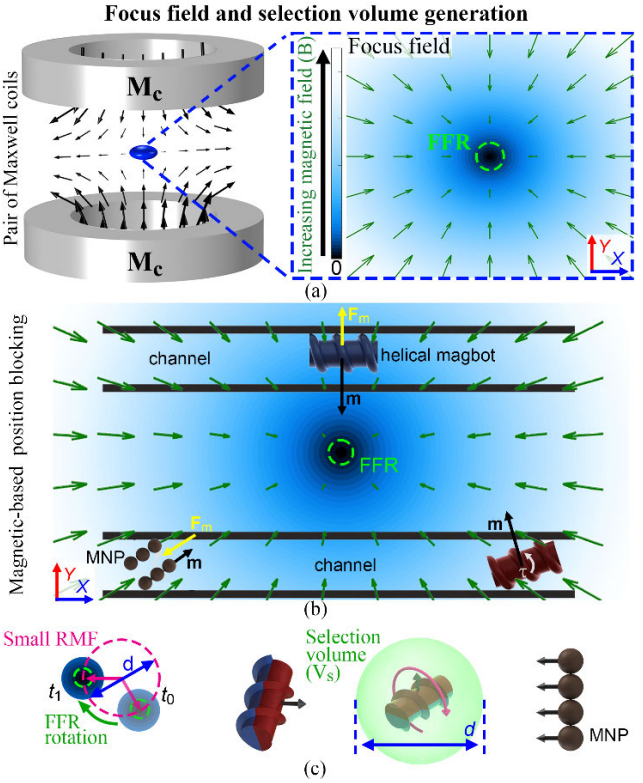

FIGURE 1. Focus field and selection volume generation. (a) A pair of Maxwell coils generating a focus field, with a region of zero magnetic field at its center (Field free region - FFR). (b) The magnetic gradient of the focus field exerts a magnetic force that pushes magbots toward the walls of channels. (c). The addition of a small uniform magnetic rotating field (RMF) displaces the FFR of the focus field and causes it to rotate describing a spherical selection volume (V_s). A magbot within V_s can fully rotate synchronizing with the applied RMF, whereas magbots outside of it cannot.

A circular pair of Maxwell coils is a set of two identical circular coils separated by a distance equal to $\sqrt{3}$ times their radius, with an electrical current I_m flowing in opposite directions. As shown in Fig. 1(a), this creates a magnetic field distribution characterized by a point of zero magnetic field (Field free region (FFR)) at the center of the pair of coils

(that coincides with the origin of the coordinate system), from which the magnetic field increases following:

$$\mathrm{FF} = \mathbf{G}\mathbf{p} \tag{1}$$

where $\mathbf{p}$ is the spatial position and the magnetic gradient tensor $\mathbf{G}$ is the diagonal matrix diag $\left[-g_z/2 \ -g_z/2 \ g_z \right]$, and g_z is the magnitude of the gradient in the Z-axis. For the pair of coils used in this electromagnetic system and axis in Z, (further detailed in a previous work [26]) the relationship between I_m and g_z is given by:

$$g_z = k_m I_m \tag{2}$$

where k_m is a constant (0.035 $\mathrm{T{\cdot}m^{-1}{\cdot}A^{-1}}$) related to the geometry of the coils.

As Fig. 1(b) shows, if an FF is applied to any type of magbot (with a magnetic moment $\mathbf{m}$) confined within channels, the magnetic gradient will exert magnetic forces ($\mathbf{F}_m = \nabla(\mathbf{B} \cdot \mathbf{m})$) that push them toward the walls of the channels in opposite radial direction from the FFR, while also exerting magnetic torques ($\tau_m = \mathbf{m} \times \mathbf{B}$) that further restrict the orientation of the magbots.

Then, by applying an RMF (generated by the Helmholtz coils) the original position of the FFR shifts (by a distance that depends on the magnitude of RMF ($\mathrm{B_{RMF}}$) and rotates creating an ellipsoidal volume, herein referred to as selection volume. The major axis d of $\mathrm{V_s}$ is:

$$d = 2\mathrm{B}_{RMF}/g_z \tag{3}$$

As depicted in Fig. 1(c), only a magbot contained within $\mathrm{V_s}$ will be able to synchronize and rotate with the applied RMF, whereas the remaining robots will at most oscillate with their $\mathbf{m}$ pointing toward FFR. So, to selectively control a given magbot $d/2$ must be smaller than the separation distance between the target magbot and the closest one to it.

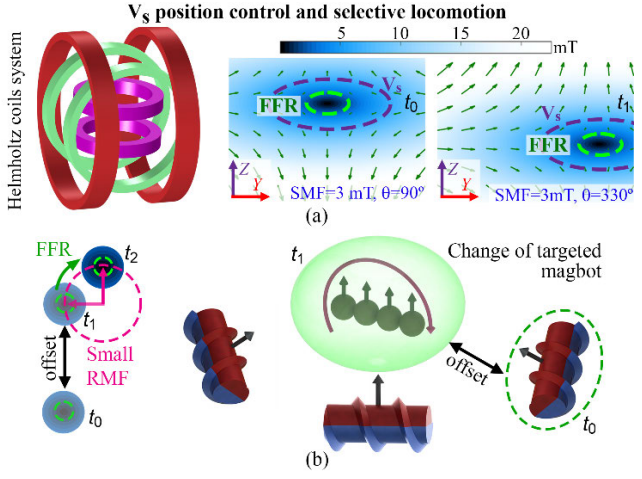

FIGURE 2. $\mathbf{V_s}$ **position control and selective locomotion. (a) A 3D set of Helmholtz coils generate time static uniform fields (SMF) that change the original position of FFR, and the center of** $\mathbf{V_s}$**. (b) By matching the center of Vs to the center of targeted magbot, several magbots can be selectively controlled.**

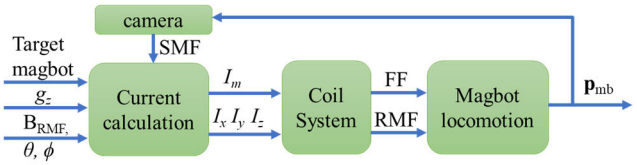

FIGURE 3. Block diagram of control system.

The next step is to control the center of $\mathrm{V_s}$. As shown in Fig. 2(a), position control of $\mathrm{V_s}$ is achieved by the addition of a quasistatic magnetic field (SMF) which is:

$$\mathrm{SMF} = -\mathbf{G}\,\mathbf{p}_{mb} \tag{4}$$

where $\mathbf{p}_{\mathrm{mb}}$ is the position toward which the center of $\mathrm{V_s}$ will be shifted to. The field generated by the pairs of Helmholtz coils is:

$$\left[B_x \ B_y \ B_z \right]^{\mathrm{T}} = \left[k_x I_x \ k_y I_y \ k_z I_z \right]^{\mathrm{T}} \tag{5}$$

where k_x ($1.76 \times 10^{-3}\,\mathrm{T{\cdot}A^{-1}}$), k_y ($1.8 \times 10^{-3}\,\mathrm{T{\cdot}A^{-1}}$) and k_z ($3.74 \times 10^{-3}\,\mathrm{T{\cdot}A^{-1}}$) are geometrical constants respectively for the pairs of Helmholtz coils in the X-, Y- and Z-axis, and I_x, I_y and I_z their respective electric currents.

Finally, selective locomotion is achieved by positioning the center of $\mathrm{V_s}$ with the center of a targeted magbot so that it is wrapped within $\mathrm{V_s}$, as shown in Fig. 2(b). Only the selected magbot can fully rotate and synchronize with an applied RMF, whereas the rest of magbots cannot. This, as long as the separation distance between the targeted magbot and its closest neighboring magbot is smaller than $d/2$. The RMF generated by the Helmholtz coils is:

$$\mathrm{RMF} = B_{RMF} \begin{bmatrix} \sin\theta\cos(\omega t) - \cos\phi\cos\theta\sin(\omega t) \\ -\cos\theta\cos(\omega t) - \cos\phi\sin\theta\sin(\omega t) \\ \sin\phi\sin(\omega t) \end{bmatrix} \tag{6}$$

where θ and ϕ are respectively the azimuthal and polar angles of the rotation axis of RMF, whereas ω is its angular frequency.

III. SELECTIVE LOCOMOTION OF TWO HELICAL SWIMMERS

To test the proposed locomotion mechanism, a controller for the selective locomotion of magnetic torque-based magbots was developed, as seen in Fig. 3. The user introduces the targeted robot, and the magnitudes g_z and $\mathrm{B_{RMF}}$ through the user interface. The locomotion angles θ and ϕ are controlled through a joystick. Then the controller calculates the required currents for the pair of Maxwell coils and the pairs of Helmholtz coils, which then generates the magnetic field distributions FF and RMF. After that the selected magbot moves changing its position $\mathbf{p}_{\mathrm{mb}}$, which is captured by a USB camera. Then, the SMF required to maintain the center of $\mathrm{V_s}$ at the center of the robot is calculated and fed into the control system.

The proposed control system was first tested with two identical (except for their color) helical magbots. The magbots were made using N35 Neodymium cylindrical magnets

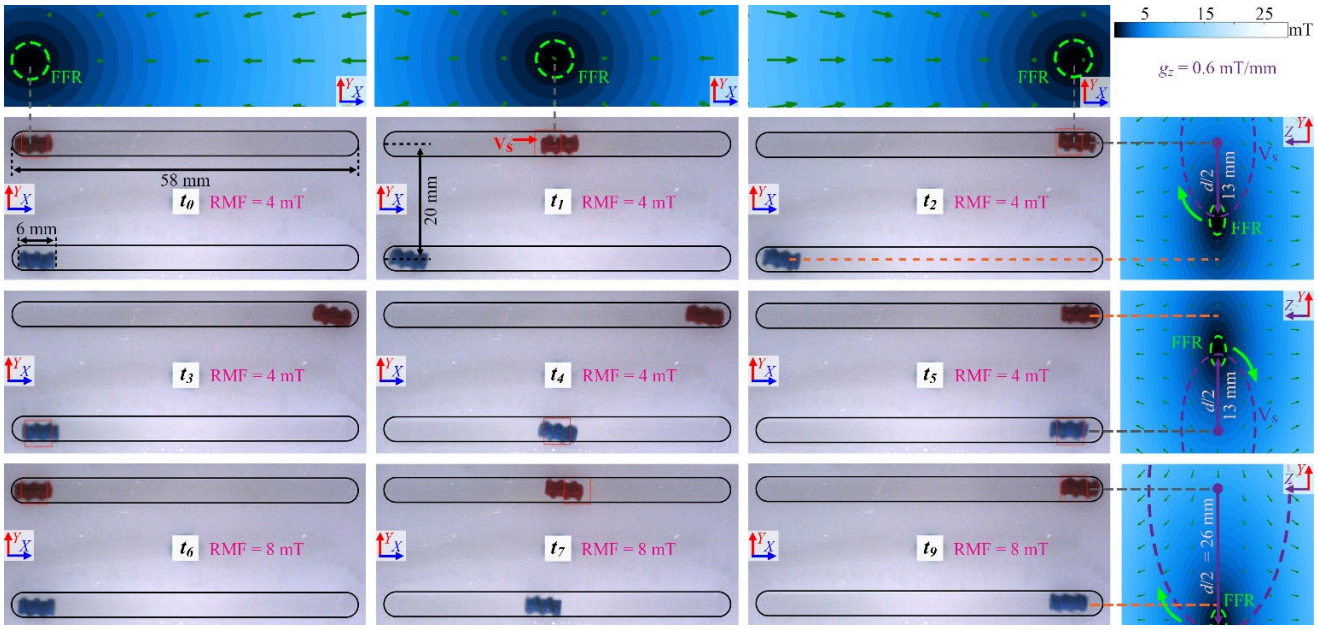

FIGURE 4. Selective locomotion of two helical magbots. From t_0 to t_2, V_S is positioned at the center of the red robot and selectively controlled from one end of the channel to the other. At t_3, V_S is changed to match the blue robot's position for its selective locomotion. The magnetic field distribution images at the XY plane show the FFR following the position of the targeted magbot. The magnetic field at ZY plane shows that from t_0 to t_5 d/2 is smaller than the separation distance between robots, hence only one robot moves; whereas from t_6 d increases and both robots move.

with respective length of 4 mm and diameter of 1.5mm. They featured a helicoidal body fabricated through a photocurable resin 3D printing process, utilizing a Micro Plus Advantage printer (EnvisionTEC, USA). The dimensions of the helicoidal body measured 6 mm in length and 3.5 mm in diameter. One magbot was painted red and the other one blue, to facilitate their tracking (see supplementary video SM1). Both magbots were placed within 4.2 mm width channels separated by a distance of 20 mm, as shown in Fig. 3. The channels were filled with a mixture of water and glycerin with a dynamic viscosity of 45.38 mPa·s. As in most research regarding magnetic milli/microrobots, the fluid's viscosity was tuned to the referred value so that the Reynolds number approached a low value (between 10^{-2} to 10^{-3}) similar to that of microorganisms [27], [28].

First, g_z was set to 0.6 mT/mm and B_{RMF} to 4 mT, resulting in a d of 26 mm. The center of V_s (marked with a red rectangle in the images and videos) was matched to the red magbot. Then the red magbot was moved from the left end of the channel (t_0) to the right end (t_2), while the blue magbot remained in its original position. As observed in the magnetic field distribution images for the *XY* plane, the original position of the FFR was adjusted to follow the targeted robot, whereas the distribution in the *ZY* plane shows that Vs only covered the red robot, being this the reason why the blue robot could not rotate and propel itself along its respective channel.

After the red robot reached the right end of its channel, the center of Vs was changed to match the blue magbot (t_3), and subsequently the targeted robot was moved toward the opposite end of the channel (t_5). As further observed in the *ZY* magnetic field distribution, V_s only wrapped the blue robot.

Then B_{RMF} was increased to 8 mT, resulting in a larger V_s with $d = 52$ mm, large enough to cover both magbots. Despite positioning the center of Vs at the red robot, it is observed that both robots moved from one end of their respective channels to the other one. This demonstrates that to ensure selective locomotion, the volume of Vs must be small enough to wrap only the targeted robot. If several robots are wrapped within Vs, selective locomotion will fail.

IV. SELECTIVE LOCOMOTION OF MNP AND SPLITTING MECHANISM

In the case of soft magnetic materials, such as magnetic nanoparticles (MNP), their **m** changes with the control magnetic fields and disappears when the fields are suppressed. Hence, the magnetic torque and force that a soft magbot experiences will depend on its relative position to the FFR. Thus, such magbots require higher magnetic gradients and magnetic fields for their locomotion. By exploiting this property, a mechanism for the splitting and distribution of magnetic swarms was developed, as shown in Fig. 5 (a). In the absence of a magnetic field, MNPs form randomly oriented clusters with a net **m** of zero.

Considering the current maximum attainable values for g_z (approximately 7 mT/mm [29]), if an FFR is placed at the center of a cluster of MNPs, the magnetic force will be negligible because **m** is almost zero. However, the addition of an RMF partially magnetizes the MNPs inside V_s, inducing the formation of magnetic chains that rotate along with the RMF, as shown in Fig. 5(b). However, in the case of swarms located outside V_s, the assembled chains do not rotate but exhibit an oscillating motion that propels the chain in the direction of the magnetic gradient. As the MNPs move further

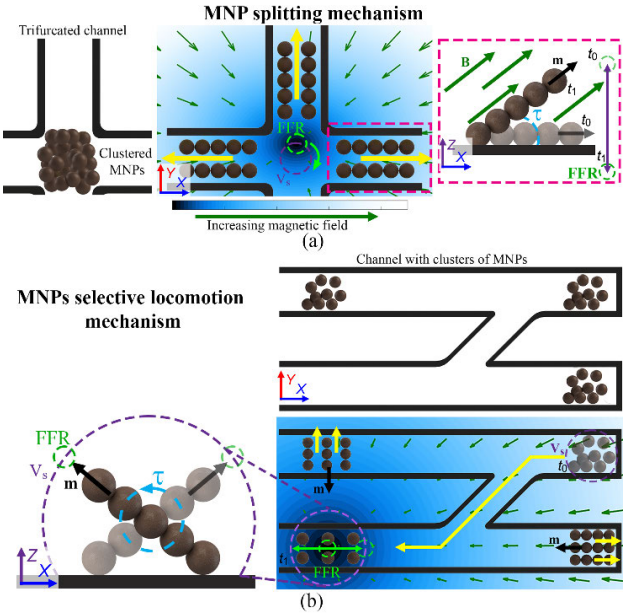

FIGURE 5. Splitting (a) and selective locomotion (b) mechanisms for magnetic nanoparticles using an FF.

away from V_s, the amplitude of the oscillation decreases, and the magnetic force becomes dominant.

The aforementioned mechanisms were tested using about 15 mg of bare spherical Fe_3O_4 MNPs with and average core size of 80-100 nm (bought from US Research Nanomaterials, Inc., TX, USA) in a 1.5 mm wide acrylic channel filled with silicone oil (dynamic viscosity of 12 mPa·s), with g_z set to 1.8 mT/mm and an B_{RMF} of 7 mT at f = 18 Hz (see supplementary video SM2).

Fig. 6 shows time-lapse images of the nonselective locomotion of the MNPs (g_z = 0 mT/mm) moving from the upper-left section to the right side of the upper channel. Although the initial volume occupied by the MNPs is small, as they move to the right, a large cloud of MNPs is created owing to the combined effect of the dragging force, capillary action, and inter-particle magnetic interactions. Then we proceeded to demonstrate the MNP swarm splitting and selective locomotion mechanisms, as shown in Fig. 7. First, the initial swarm was moved approximately 6 mm to the left (t_0–t_2), so that it expanded. The FF was then applied, and the FFR was placed at the center of the MNP cloud, dividing the original swarm into two (t_3), as observed in Fig. 7(a).

Subsequently, V_s was positioned over the swarm on the right side (t_4) and was controlled following the trajectory described with yellow arrows toward the targeted region (t_5), as shown in Fig. 7(b). Then, the other magnetic swarm located in the upper section was targeted (t_6) and controlled toward the selection region located on the left lower side of the channel (t_7). Finally, the magnetic swarm was split once again into two, one of which was targeted and selectively controlled toward the targeted region located in the central lower region of the channel. Finally, each of the three targeted regions contained MNPs, which were initially part of a single swarm of MNPs.

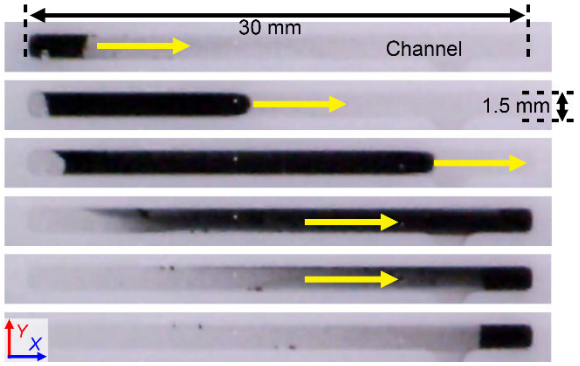

FIGURE 6. Non-selective locomotion of MNPs.

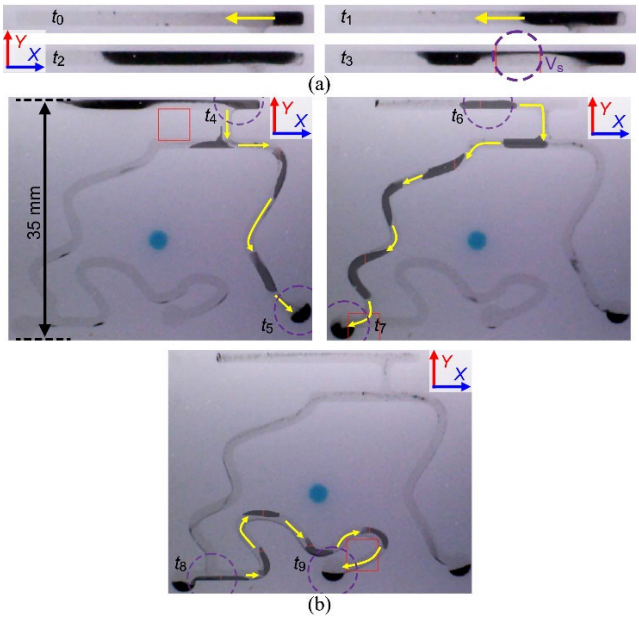

FIGURE 7. Experimental demonstration of splitting (a) and selective locomotion (b) mechanisms for MNPs.

V. SELECTIVE CONTROL OF HETEROGENEOUS MAGBOTS AND POTENTIAL APPLICATIONS

The proposed system can be used to selectively control task-specific tailored heterogeneous magbots, allowing them to perform several applications at once, such as the drilling of clots, targeted delivery, and delivery-retrieval of MNPs. To exemplify this, we performed selective control of two identical magbots (MB_1 and MB_2) and magnetic particles (NdFeB powder, approximately 10 mg) inside an acrylic channel filled with a water-glycerin mix for the drilling of agar jellies (J_1 and J_2), targeted delivery of lead balls (B_1 and B_2) and magnetic powder, and retrieval of magnetic particles, as shown in Fig. 8(a) (see supplementary video SM3). Magbots MB_1 and $MB_2$are comprised of cylindrical neodymium magnets, each with a diameter of 0.8 mm and a length of 3 mm. A copper wire, with a 0.2 mm diameter, was coiled around these magnets, imparting a helical shape. Subsequently, MB_1 and MB_2 were respectively decorated with red and blue colors, for identification.

First, as shown in Fig. 8(b), MB_2 (blue) was selectively controlled and moved from its original position (t_0) toward J_1.

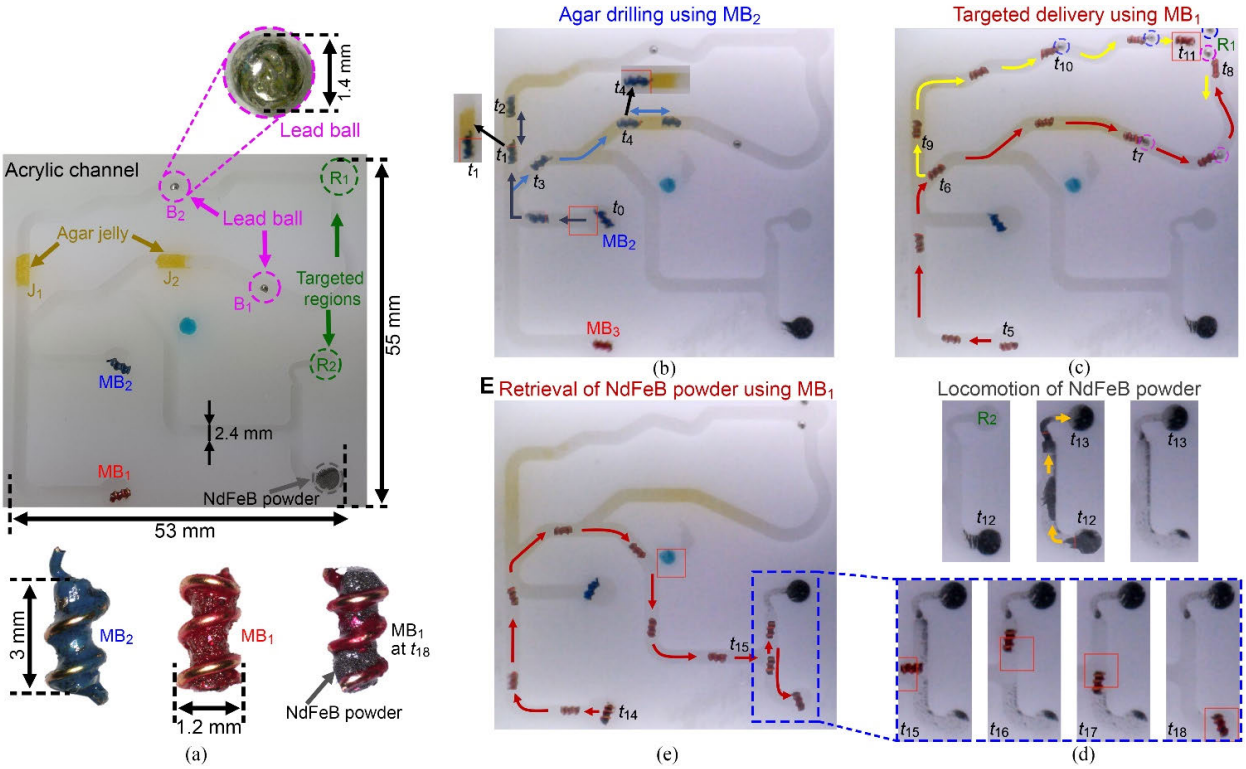

FIGURE 8. Selective control of heterogeneous magnetic robots. (a) Experimental set comprising two different functions using MB_1 and MB_2, lead balls (B_1 and B_2), NeFeB powder, and agar jellies (J_1 and J_2), inside an acrylic channel. In the lower section, a close-up picture of MB_2, and MB_1 before and after retrieval of NdFeB powder, respectively. (b) Time-lapse images of drilling of the agar jellies through the selective control of MB_2. (c) Time-lapse images of the delivery of the lead balls toward the targeted regions R_1, through the selective control of MB_1. (d) Time-lapse images of the selective locomotion of NeFeB powder toward the targeted region R_2. (e) Retrieval of NeFeB powder located outside the targeted region R_2, through the selective control of MB_1.

After MB_2 reached J_1 (t_1), it started an upward and downward motion across J_1 until the jelly was completely dissolved (t_2). It then moved toward J_2 (t_3–t_4) and performed a forward and backward motion across J_2 until the jelly dissolved, after which MB_2 was moved back to its original position. Then, MB_1 (red) was controlled following the red arrow trajectory (t_5) toward B_1 (magenta circled) and pushed to the targeted region R_1 (t_7–t_8), as shown in Fig. 8(c). Subsequently, MB_1returned following the same trajectory until it reached the upper bifurcation on the left side of the channel, following the yellow line trajectory toward B_2 (blue circles), and pushed to the targeted region R_1(t_{10}–t_{11}), after which MB_1 returned to its starting position.

Then, $V_s$was positioned over the NeFeB powder (t_{12}), and the control type was changed for the locomotion of MNPs. Subsequently, the powder was moved upward toward the targeted region R_2 while leaving behind some magnetic powder (t_{12}–t_{13}), as shown in Fig. 8(d). Next, $MB_1$was selectively controlled toward the region where the magnetic powder was actuated (t_{14}–t_{15}) following the red arrow trajectory (Fig. 8(e)) to retrieve the remnant magnetic powder located outside R_2, as shown in time-lapse images from t_{15} to t_{18}. The appearance of MB_1 with the attached magnetic powder is shown in the lower part of Fig. 8(a).

When MNPs are exposed to magnetic fields on the order of kilohertz, they produce a significant amount of heat, which is deemed suitable for hyperthermia applications (i.e., thermal therapy for cancer). In previous research, the FF has been used to confine the heating of MNPs to the area within the vicinity of the FFR to improve selectivity during hyperthermia [26], [30]; however, if the number of MNPs in the targeted region is scarce, the temperature in this region will not increase to the required value.

Using our proposed selective control mechanism for MNPs, the MNP swarms can be redistributed throughout the body to control the maximum temperature reached during magnetic heating. To demonstrate this, we placed approximately 30 mg of Fe_3O_4 MNPs at the center of a silicone oil-filled acrylic channel that diverges from the center into three equidistantly separated channels, to perform selective locomotion and heating applications, as shown in Fig. 9 (see supplementary video SM4).

First, g_z was set 1.8 mT/mm and the center of V_s was matched to the position of the MNPs. Subsequently, an RMF with B_{RMF} of 8 mT and a frequency of 18 Hz was applied. As soon as the RMF was applied, the MNPs started to oscillate and move along the three channels toward the three targeted points, P1 to P3, as shown in the time-lapse images (t_0–t_4) of Fig. 9(a). Then, the FF and RMF were turned off, and a high-frequency field (16 kA/m, 200 kHz) was arbitrarily applied for 100 s. Based on the thermal images (Fig. 9(c)), the temperature increased from 18.5°, 18.4°, and 19.4° C (t_4)

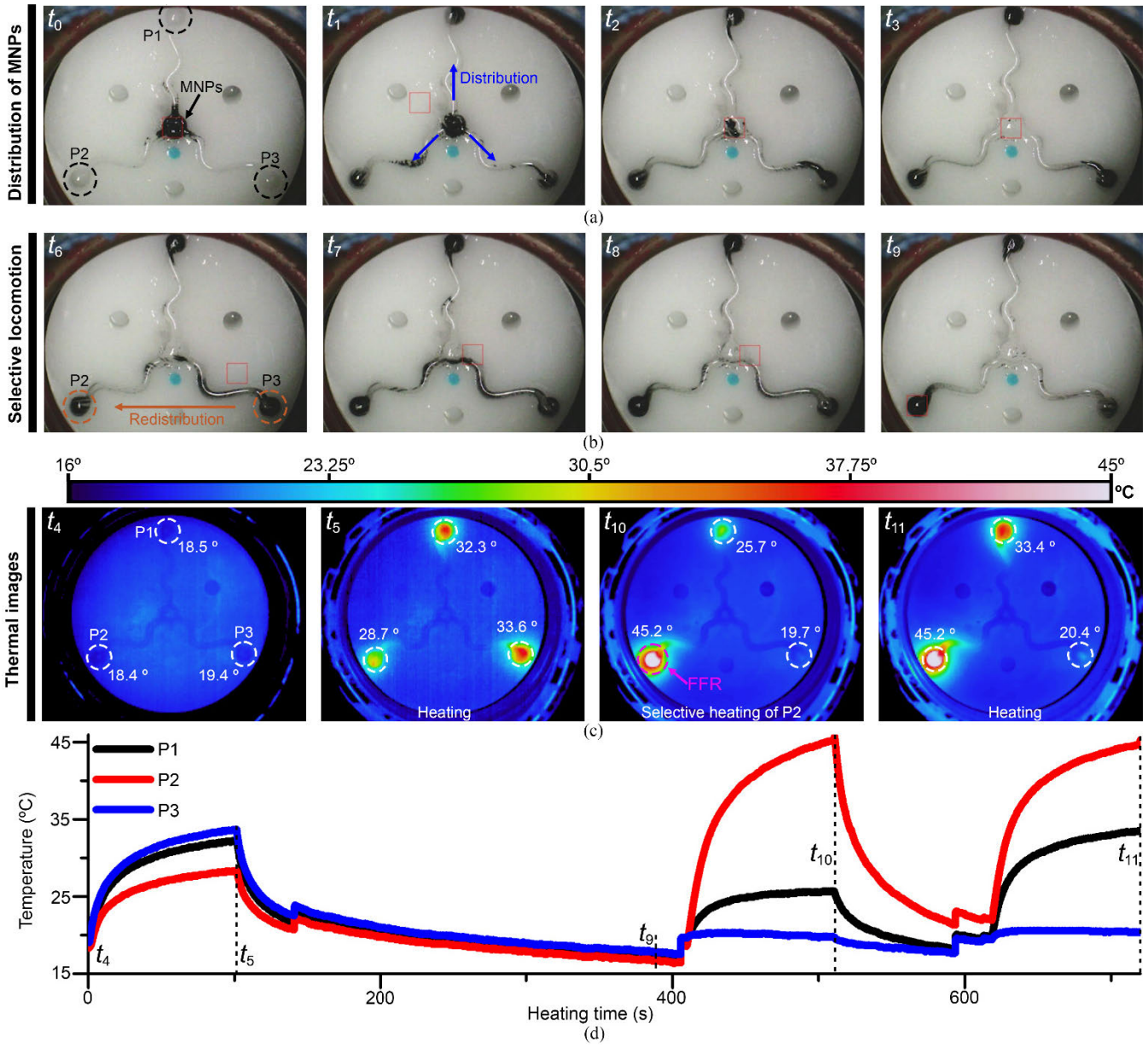

FIGURE 9. Selective locomotion and heating of MNPs. (a) Time-lapse images of the distribution of MNPs from the center of the channel to three equidistant targeted points (P1 to P3). (b) Time-lapse images of the selective locomotion of MNPs located at P3 toward P1. (c) Thermal images of the uniform (t_4- after distribution of MNPs but before heating, and t_5- after heating for 100 s) and selective heating for 100 s of MNPs within the channel before (t_{10}) and after (t_{11}) the selective locomotion of MNPs from P3 to P1. (d) Graph of the average temperature of the three targeted regions during the different heating and locomotion conditions.

to 32.3°, 28.7° and 33.6° C (t_5), respectively, for P1 to P3. The graph in Fig. 9(d) shows the measured temperatures for each of the three targeted points during the heating experiments (t_4–t_{11}), starting after the high frequency was first turned on. With the objective of increasing the temperature of P2 to approximately 43° C while suppressing the heat in the other two regions, the MNPs located at P3 were moved to P2 (t_6–t_9), as shown in the time-lapse image of Fig. 9(b).

As observed, the MNPs at P1 did not change their position, whereas most MNPs from P3 were successfully moved to P2. Subsequently, without turning off the FF whose center was at P2, a high-frequency magnetic field was applied again for 100s. As the thermal image (t_{10}) shows, the temperature at P2 rose significantly to 45.2° C due to the increased amount of MNPs, whereas the temperature at P1 barely increased to 25.7° C as a result of the MNPs of P1 being partially magnetized by the FF. Moreover, the temperature at P3 did not increase owing to the absence of the MNPs.

After cooling for approximately 200s, the high-frequency magnetic field was applied again for 100s, while the FF was turned off, resulting in P3 increasing again to 45.2° C and P1 to 33.4° C—almost the same as the first heating cycle.

This was expected because the number of MNPs at P1 did not change with respect to the first heating cycle.

VI. CONCLUSION

Herein, we introduce a novel control mechanism that uses only global magnetic fields for the selective locomotion of magnetic torque-based magbots, especially when these are confined within channels. This system leverages a unique magnetic gradient distribution termed the ''focus field'' (FF). A defining feature of FF is the presence of a field free region (FFR) at its center. The FF exerts magnetic forces and torques that block the position of channel confined magbots that are located far from the FFR and prevent them from aligning with other applied magnetic fields. The addition of an RMF results in a displacement and rotation of the FFR, delimiting a V_s within which magbots can fully rotate, whereas magbots outside of it cannot. Hence, this method selectively ''switches on'' and ''off'' the propulsion of magnetic torque-based magbots.

Historically, control strategies have predominantly employed identical or near-identical magbots, meaning slight variations existed between individual magbots. As a result, if one needs to switch the type of magbot for a different task, all magbots in the operational space must first be removed. Furthermore, modifications to the control system might be necessary. This limitation is overcome by our introduced selective control mechanism. Sections III and IV empirically validate the capability of our proposed mechanism to function with heterogeneous magbots, encompassing diverse geometrical and magnetic properties like permanent magnet-based helical magbots and magnetic nanoparticles (MNPs). To our knowledge, this is the first demonstration of such capability. Our experimental results corroborate that when one set of magbots (either helical or MNP swarm) is selectively activated, the others remain stationary.

Although our experiments involving helical magbots were conducted with only two units, the same system is scalable for controlling a more significant number of magbots. While this selective locomotion mechanism facilitates 3D control, an augmented tracking methodology (potentially ultrasound) would enhance accuracy, especially given the overlapping issues of the robots during dual-camera (planes *XY* and *ZY*) tracking.

In experiments involving pairs of orthogonal coils, when two swarms of MNPs converge, they amalgamate, making it challenging to separate them subsequently. While some recent studies have successfully disintegrated the MNP swarms using alternative configurations of RMF [31], [32], these techniques have notable limitations. Specifically, these methods consume a considerable amount of time (approximately one minute), indiscriminately disperse all the existing swarms within the operational space, and lack the capacity to control the swarms independently. Moreover, once the locomotion fields are reintroduced, the swarms tend to coalesce once more. Contrastingly, as we have experimentally showcased in section IV, our proposed control system offers a more suitable approach. It allows for the selective and quicker (within 20 seconds) bifurcation of MNP swarms. Additionally, it provides the capability for selective actuation of the swarms. Such advancements are pivotal in enhancing the controllability and efficiency of in-vivo applications like selective embolization [1] and targeted annihilation of cancer cells [33]. The efficacy of this approach was further validated through our optimized selective heating strategy, as detailed in section V.

Recent studies have provided evidence that helical and rolling magbots are capable of moving against flow rates up to 32 mm/s and 6 mm/s, respectively [34], [35]. This suggests the potential applicability of this control method in vascular environments characterized by low blood flow, such as cerebral capillaries [36]. Nonetheless, the integration of rapid tracking technologies, including ultrasound or optoacoustic imaging, is a prerequisite to fully realize this potential. In our subsequent research, the focus will be directed towards the incorporation of these tracking modalities and enhancing the proposed selective locomotion mechanism to facilitate its in-vivo implementation.

REFERENCES

[1] J. Law, X. Wang, M. Luo, L. Xin, X. Du, W. Dou, T. Wang, G. Shan, Y. Wang, P. Song, X. Huang, J. Yu, and Y. Sun, ''Microrobotic swarms for selective embolization,'' *Sci. Adv.*, vol. 8, no. 29, Jul. 2022, Art. no. eabm5752, doi: 10.1126/sciadv.abm5752.

[2] M. Luo, J. Law, X. Wang, L. Xin, G. Shan, M. Badiwala, X. Huang, and Y. Sun, ''Robotic swarm control for precise and on-demand embolization,'' in *Proc. IEEE Int. Conf. Robot. Autom. (ICRA)*, May 2020, pp. 4470–4476, doi: 10.1109/ICRA40945.2020.9197009.

[3] L. Zheng, S. Guo, and M. Kawanishi, ''Magnetically controlled multifunctional capsule robot for dual-drug delivery,'' *IEEE Syst. J.*, vol. 16, no. 4, pp. 6413–6424, Dec. 2022, doi: 10.1109/JSYST.2022.3145869.

[4] X. Chen, C. Tian, H. Zhang, and H. Xie, ''Biodegradable magnetic hydrogel robot with multimodal locomotion for targeted cargo delivery,'' *ACS Appl. Mater. Interfaces*, vol. 15, no. 24, pp. 28922–28932, Jun. 2023, doi: 10.1021/acsami.3c02703.

[5] R. H. Soon, Z. Yin, M. A. Dogan, N. O. Dogan, M. E. Tiryaki, A. C. Karacakol, A. Aydin, P. Esmaeili-Dokht, and M. Sitti, ''Pangolin-inspired untethered magnetic robot for on-demand biomedical heating applications,'' *Nature Commun.*, vol. 14, no. 1, Jun. 2023, doi: 10.1038/s41467-023-38689-x.

[6] A. Ahmed, E. Kim, S. Jeon, J. Kim, and H. Choi, ''Closed-loop temperature-controlled magnetic hyperthermia therapy with magnetic guidance of superparamagnetic iron-oxide nanoparticles,'' *Adv. Therapeutics*, vol. 5, no. 2, Feb. 2022, Art. no. 2100237, doi: 10.1002/adtp.202100237.

[7] S. Kim, S. Bae, W. Lee, and G. Jang, ''Magnetic navigation system composed of dual permanent magnets for accurate position and posture control of a capsule endoscope,'' *IEEE Trans. Ind. Electron.*, vol. 71, no. 1, pp. 1–9, Jan. 2023, doi: 10.1109/TIE.2023.3245195.

[8] D. Son, M. C. Ugurlu, and M. Sitti, ''Permanent magnet array-driven navigation of wireless millirobots inside soft tissues,'' *Sci. Adv.*, vol. 7, no. 43, Oct. 2021, Art. no. abi8932, doi: 10.1126/sciadv.abi8932.

[9] M. Yousefi and H. Nejat Pishkenari, ''Independent position control of two identical magnetic microrobots in a plane using rotating permanent magnets,'' *J. Micro-Bio Robot.*, vol. 17, no. 1, pp. 59–67, Jan. 2021, doi: 10.1007/s12213-021-00143-w.

[10] A. Ramos-Sebastian and S. H. Kim, ''Magnetic force-propelled 3D locomotion control for magnetic microrobots via simple modified three-axis Helmholtz coil system,'' *IEEE Access*, vol. 9, pp. 128755–128764, 2021, doi: 10.1109/ACCESS.2021.3113765.

[11] D. Li, F. Niu, J. Li, X. Li, and D. Sun, ''Gradient-enhanced electromagnetic actuation system with a new core shape design for microrobot manipulation,'' *IEEE Trans. Ind. Electron.*, vol. 67, no. 6, pp. 4700–4710, Jun. 2020, doi: 10.1109/TIE.2019.2928283.

[12] L. Yang, X. Du, E. Yu, D. Jin, and L. Zhang, ''DeltaMag: An electromagnetic manipulation system with parallel mobile coils,'' in *Proc. Int. Conf. Robot. Autom. (ICRA)*, Montreal, QC, Canada, May 2019, pp. 9814–9820, doi: 10.1109/ICRA.2019.8793543.

[13] A. Ramos-Sebastian, S. Hwang, and S. H. Kim, "Single coil mechano-electromagnetic system for the automatic 1-axis position feedback 3D locomotion control of magnetic robots and their selective manipulation," *Adv. Sci.*, vol. 9, no. 23, Aug. 2022, Art. no. 2201968, doi: 10.1002/advs.202201968.

[14] L. Yang and L. Zhang, "Motion control in magnetic microrobotics: From individual and multiple robots to swarms," *Annu. Rev. Control, Robot., Auto. Syst.*, vol. 4, no. 1, pp. 509–534, May 2021, doi: 10.1146/annurev-control-032720-104318.

[15] G. Cui, P. Zhang, X. Liu, L. Xie, W. Huang, P. Pan, J. Qu, and Q. Fan, "Novel coil array design and modeling for independent control of multiple magnetic microrobots," *IEEE Trans. Ind. Electron.*, vol. 70, no. 10, pp. 10302–10311, Oct. 2023, doi: 10.1109/TIE.2022.3222626.

[16] Y. Kantaros, B. V. Johnson, S. Chowdhury, D. J. Cappelleri, and M. M. Zavlanos, "Control of magnetic microrobot teams for temporal micromanipulation tasks," *IEEE Trans. Robot.*, vol. 34, no. 6, pp. 1472–1489, Dec. 2018, doi: 10.1109/TRO.2018.2861901.

[17] J. Giltinan, P. Katsamba, W. Wang, E. Lauga, and M. Sitti, "Selectively controlled magnetic microrobots with opposing helices," *Appl. Phys. Lett.*, vol. 116, no. 13, Mar. 2020, Art. no. 134101, doi: 10.1063/1.5143007.

[18] E. Diller, S. Floyd, C. Pawashe, and M. Sitti, "Control of multiple heterogeneous magnetic microrobots in two dimensions on nonspecialized surfaces," *IEEE Trans. Robot.*, vol. 28, no. 1, pp. 172–182, Feb. 2012, doi: 10.1109/TRO.2011.2170330.

[19] T. Xu, C. Huang, Z. Lai, and X. Wu, "Independent control strategy of multiple magnetic flexible millirobots for position control and path following," *IEEE Trans. Robot.*, vol. 38, no. 5, pp. 2875–2887, Oct. 2022, doi: 10.1109/TRO.2022.3157147.

[20] E. Diller, S. Miyashita, and M. Sitti, "Magnetic hysteresis for multi-state addressable magnetic microrobotic control," in *Proc. IEEE/RSJ Int. Conf. Intell. Robots Syst.*, Oct. 2012, pp. 2325–2331, doi: 10.1109/IROS.2012.6386010.

[21] S. Kim, M. Cho, S. Im, J. Yun, and J. Nam, "Electrical optimization method based on a novel arrangement of the magnetic navigation system with gradient and uniform saddle coils," *Sensors*, vol. 22, no. 15, p. 5603, Jul. 2022, doi: 10.3390/s22155603.

[22] Q. Zhang, S. Song, P. He, H. Li, H.-Y. Mi, W. Wei, Z. Li, X. Xiong, and Y. Li, "Motion control of magnetic microrobot using uniform magnetic field," *IEEE Access*, vol. 8, pp. 71083–71092, 2020, doi: 10.1109/ACCESS.2020.2986089.

[23] M. Abdelaziz and M. Habib, "Electromagnetic actuation for a micro/nano robot in a three-dimensional environment," *Micromachines*, vol. 13, no. 11, p. 2028, Nov. 2022, doi: 10.3390/mi13112028.

[24] J. Rahmer, C. Stehning, and B. Gleich, "Spatially selective remote magnetic actuation of identical helical micromachines," *Sci. Robot.*, vol. 2, no. 3, Feb. 2017, Art. no. aal2845, doi: 10.1126/scirobotics.aal2845.

[25] K. Bente, A. C. Bakenecker, A. von Gladiss, F. Bachmann, A. Cebers, T. M. Buzug, and D. Faivre, "Selective actuation and tomographic imaging of swarming magnetite nanoparticles," *ACS Appl. Nano Mater.*, vol. 4, no. 7, pp. 6752–6759, Jul. 2021, doi: 10.1021/acsanm.1c00768.

[26] A. Ramos-Sebastian, S. Gwak, and S. H. Kim, "Multimodal locomotion and active targeted thermal control of magnetic agents for biomedical applications," *Adv. Sci.*, vol. 9, no. 7, Mar. 2022, Art. no. 2103863, doi: 10.1002/advs.202103863.

[27] J. J. Abbott, K. E. Peyer, M. C. Lagomarsino, L. Zhang, L. Dong, I. K. Kaliakatsos, and B. J. Nelson, "How should microrobots swim?" *Int. J. Robot. Res.*, vol. 28, no. 11, pp. 1434–1447, Jul. 2009, doi: 10.1177/0278364909341658.

[28] G. Kararsiz, Y. C. Duygu, Z. Wang, L. W. Rogowski, S. J. Park, and M. J. Kim, "Navigation and control of motion modes with soft microrobots at low Reynolds numbers," *Micromachines*, vol. 14, no. 6, p. 1209, Jun. 2023, doi: 10.3390/mi14061209.

[29] S.-M. Choi, J.-C. Jeong, J. Kim, E.-G. Lim, C.-B. Kim, S.-J. Park, D.-Y. Song, H.-J. Krause, H. Hong, and I. S. Kweon, "A novel three-dimensional magnetic particle imaging system based on the frequency mixing for the point-of-care diagnostics," *Sci. Rep.*, vol. 10, no. 1, p. 11833, Jul. 2020, doi: 10.1038/s41598-020-68864-9.

[30] Z. W. Tay, P. Chandrasekharan, A. Chiu-Lam, D. W. Hensley, R. Dhavalikar, X. Y. Zhou, E. Y. Yu, P. W. Goodwill, B. Zheng, C. Rinaldi, and S. M. Conolly, "Magnetic particle imaging-guided heating in vivo using gradient fields for arbitrary localization of magnetic hyperthermia therapy," *ACS Nano*, vol. 12, no. 4, pp. 3699–3713, Mar. 2018, doi: 10.1021/acsnano.8b00893.

[31] G. Gardi, S. Ceron, W. Wang, K. Petersen, and M. Sitti, "Microrobot collectives with reconfigurable morphologies, behaviors, and functions," *Nature Commun.*, vol. 13, p. 2239, Apr. 2022, doi: 10.1038/s41467-022-29882-5.

[32] M. Li, T. Zhang, X. Zhang, J. Mu, and W. Zhang, "Vector-controlled wheel-like magnetic swarms with multimodal locomotion and reconfigurable capabilities," *Frontiers Bioeng. Biotechnol.*, vol. 10, Apr. 2022, Art. no. 877964, doi: 10.3389/fbioe.2022.877964.

[33] Y. Shen, W. Zhang, G. Li, P. Ning, Z. Li, H. Chen, X. Wei, X. Pan, Y. Qin, B. He, Z. Yu, and Y. Cheng, "Adaptive control of nanomotor swarms for magnetic-field-programmed cancer cell destruction," *ACS Nano*, vol. 15, no. 12, pp. 20020–20031, Nov. 2021, doi: 10.1021/acsnano.1c07615.

[34] Q. Wang, X. Du, D. Jin, and L. Zhang, "Real-time ultrasound Doppler tracking and autonomous navigation of a miniature helical robot for accelerating thrombolysis in dynamic blood flow," *ACS Nano*, vol. 16, no. 1, pp. 604–616, Jan. 2022, doi: 10.1021/acsnano.1c07830.

[35] Q. Wang, Y. Tian, X. Du, H. Ko, B. Y. M. Ip, T. W. H. Leung, S. C. H. Yu, and L. Zhang, "Magnetic navigation of collective cell microrobots in blood under ultrasound Doppler imaging," *IEEE/ASME Trans. Mechatronics*, vol. 27, no. 5, pp. 3174–3185, Oct. 2022, doi: 10.1109/TMECH.2021.3109346.

[36] P. Wrede, O. Degtyaruk, S. K. Kalva, X. L. Deán-Ben, U. Bozuyuk, A. Aghakhani, B. Akolpoglu, M. Sitti, and D. Razansky, "Real-time 3D optoacoustic tracking of cell-sized magnetic microrobots circulating in the mouse brain vasculature," *Sci. Adv.*, vol. 8, no. 19, May 2022, Art. no. abm9132, doi: 10.1126/sciadv.abm9132.

ARMANDO RAMOS-SEBASTIAN (Member, IEEE) received the B.S. degree in bionics engineering from Instituto Politécnico Nacional (IPN), Mexico City, Mexico, in 2016, the M.S. degree in electronics convergence engineering from Wonkwang University, Iksan, South Korea, in 2020, and the Ph.D. degree in convergence technology engineering from Jeonbuk National University, Jeonju, South Korea, in 2023.

He is currently a Postdoctoral Researcher with the Sejong Research and Business Foundation, Korea University, Sejong, South Korea. His current research interests include the design and control of magnetic microrobots for targeted drug delivery, magnetic hyperthermia, and magnetic particle imaging.

WONSUK JUNG received the B.S., M.S., and Ph.D. degrees in mechanical engineering from KAIST, Daejeon, South Korea, in 2008, 2010, and 2014, respectively.

He is currently a Professor with the School of Mechanical Engineering, Chungnam National University, Daejeon. His research interests include robot systems and nano/micro fabrication.

SUNG HOON KIM (Member, IEEE) received the B.S. degree in electronic engineering from Yeungnam University, Gyeongsan, South Korea, in 2005, the M.S. degree in medical and biological engineering from Kyungpook National University, Daegu, South Korea, in 2007, and the Ph.D. degree in electrical communication engineering from Tohoku University, Sendai, Japan, in 2012.

He is currently an Associate Professor with the Department of Electronics and Information Engineering, Korea University, Sejong, South Korea. His research interests include magnetic sensors and actuators, multiscale magnetic micro/nano systems, magnetic hyperthermia, and implantable medical devices.